

*Chapter 3*

Thiolate Hydrogen Bonding Mutants: Thermodynamics

### 3.1 Abstract

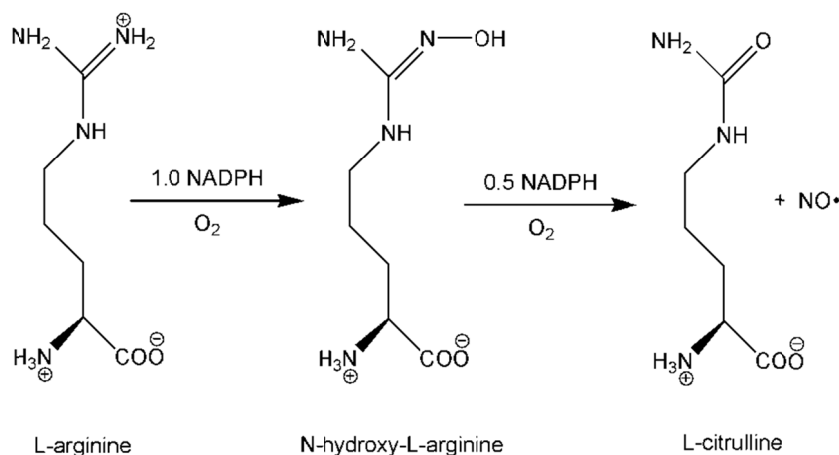
All heme thiolate enzymes have conserved hydrogen bonding networks surrounding the axial thiolate ligand. In order to understand the role of this proximal hydrogen bonding network in nitric oxide synthases, three mutants of the NOS enzyme from *Geobacillus stearothermophilus* were expressed and characterized. The wild type enzyme has a tryptophan residue at position 70 that  $\pi$ -stacks with the porphyrin ring and donates a long hydrogen-bonding interaction to the thiolate ligand of the heme iron. The native Trp was replaced with His, Phe, and Tyr. These three residues were selected to investigate the two effects of the Trp, H-bonding and  $\pi$ -stacking. Several different spectroscopic techniques were used to investigate the stability and properties of these mutant enzymes. The identity of each mutant was confirmed by mass spectrometry. Both UV-visible absorption and circular dichroism spectroscopies were used to assess the stability of the new proteins. It was shown using binding assays, generation of the ferrous-CO species, and redox titrations that the  $\sigma$ -donating abilities of the thiolate are increased after removal of the hydrogen bonding group in the Trp. Finally, electron paramagnetic resonance spectroscopy and Evans method nuclear magnetic resonance spectroscopy were used to characterize the spin state of the iron center in each mutant, reflecting the increased  $\sigma$ -donating capabilities of the thiolate upon removal of the hydrogen bonding group. The reduction potential of wild type and W70H were determined by chemical titration to be -362 and -339 mV vs. NHE, respectively. This is the first report of the reduction potential of any bacterial nitric oxide synthase.

### 3.2 Introduction

Heme-thiolate enzymes play important roles in human physiology such as drug metabolism and in the production of signaling molecules involved in processes such as neurotransmission.<sup>1-2</sup> Cytochromes P450 (cyt. P450) are a super-family of these interesting heme enzymes and many different forms are found in mammals.<sup>3</sup> They carry out a broad array of biological transformations from epoxidation of alkenes to isomerizations and many different oxidation and reduction reactions. They are most famous for their ability to hydroxylate unactivated carbon-hydrogen bonds. It would take a unique and highly reactive complex to afford such difficult and varied reactions.

There are only a small number of heme-thiolate enzymes (counting cyt. P450 as a single entity).<sup>3</sup> Joining cyt. P450 are the nitric oxide synthases (NOS) and chloroperoxidase (CPO). CPO carries out the typical peroxidase and catalase activities of any standard peroxidase enzyme.<sup>4</sup> It is unique among peroxidases, however, in its ability to use hydrogen peroxide to oxidize the halogens iodide, bromide, and chloride, and use them to form carbon-halogen bonds on substrates.

The family of enzymes called nitric oxide synthases (NOSs) is responsible for biological production of NO.<sup>5</sup> This family includes three isoforms named for the tissues in which they are found: endothelial NOS (eNOS), neuronal (nNOS), and an inducible form found in macrophages (iNOS). The function of eNOS and nNOS is regulated by calcium ions and a calmodulin linker, while the inducible isoform is calcium ion independent.<sup>6</sup> NOSs catalyze the oxidation of L-arginine (Arg) to L-citrulline in two turnovers, with N<sup>o</sup>-hydroxy-L-arginine (NOHA) as an intermediate (the product of the first turnover).<sup>7</sup> The overall reaction is shown in **Scheme 3.1**.



**Scheme 3.1:** The five-electron oxidation of arginine to form NO and citrulline.

All three isoforms are found as homodimers, each monomer consisting of an oxygenase domain and a reductase domain.<sup>8</sup> The reductase domain binds flavin adenine dinucleotide (FAD) and flavin mononucleotide (FMN) which shuttle electrons from nicotinamide adenine dinucleotide phosphate (NADPH),<sup>9</sup> the ultimate source of electrons for the reaction, to the oxygenase domain where substrate oxidation occurs. The oxygenase domain contains a thiolate-ligated heme group (protoporphyrin IX) like that in cytochromes P450 and the cofactor (6R)-5,6,7,8-tetrahydrobiopterin (pterin, H<sub>4</sub>B).<sup>8</sup> This domain successfully forms NO when supplied with a source of electrons (e.g., NADPH),<sup>10</sup> but the pterin cofactor is needed for catalysis.<sup>11-12</sup> No crystal structure for a full-length NOS has been reported, but several structures of each domain of many isoforms have been published separately.<sup>13-14</sup>

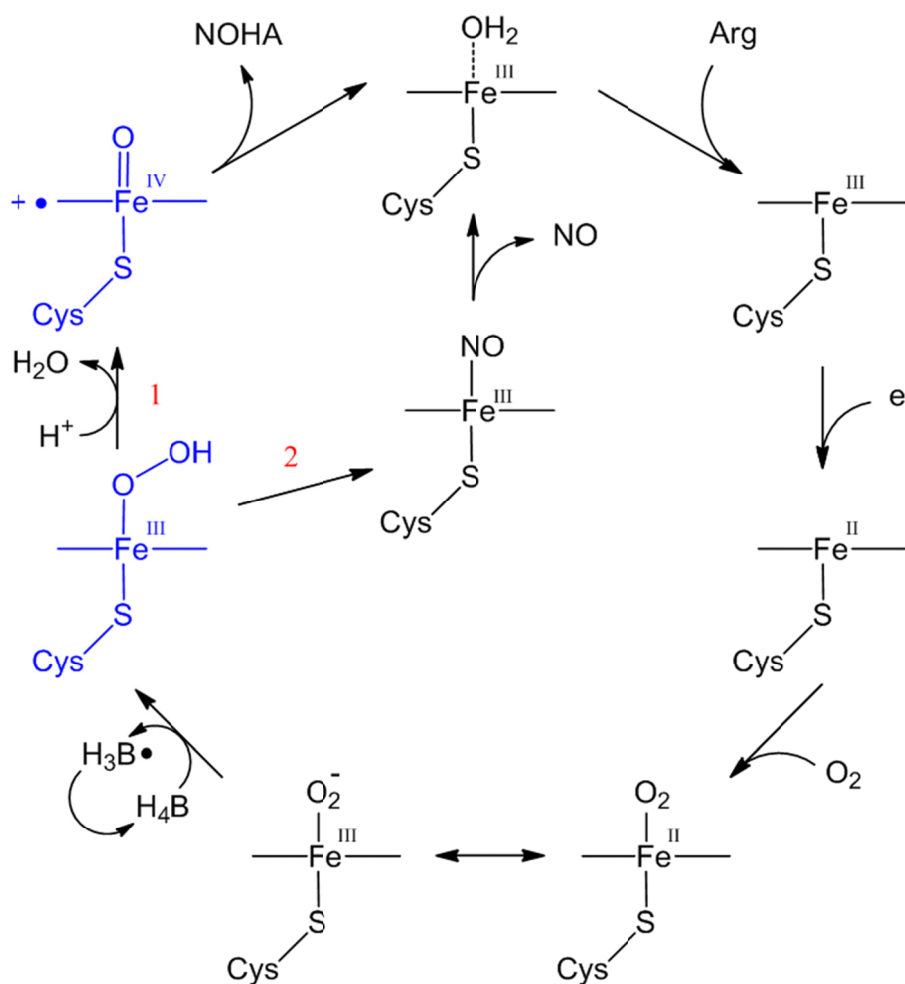
The mechanism of NOS is not fully understood.<sup>15</sup> The resting state of the enzyme is ferric heme with a water molecule occupying the sixth ligand position (four positions are occupied by the porphyrin, one by an axial cysteine, Cys194).<sup>16</sup> Catalysis begins with the binding of the substrate in both turnovers. This displaces the water molecule, but neither Arg nor NOHA ligates the heme. Binding events shift the Soret band

(characteristic absorbance of metalloporphyrins, 421 nm for substrate- and pterin-free iNOS)<sup>17</sup> as well as the spin-state (from low- to high-spin ferric).<sup>18</sup> The Soret of pterin- and arginine-loaded iNOS occurs at 390 nm. This is followed by a one-electron reduction of the iron to ferrous. Ferrous heme readily binds oxygen, forming a ferrous-oxy species (equivalent to ferric-superoxide),<sup>8</sup> the last observed intermediate in the catalytic cycle.<sup>8,19</sup>

The role pterin has been extensively investigated.<sup>11, 16, 20</sup> This molecule binds in a pocket alongside the heme, forming hydrogen bonds with a carboxylate group on the heme directly coupling it to the iron active site.<sup>13</sup> It is known that a pterin-based radical forms and is reduced during the cycle (**Scheme 3.2**), as determined by rapid-freeze electron paramagnetic resonance experiments.<sup>12, 21</sup> The current hypothesis is that proton-coupled electron transfer from pterin aids in formation of the hydroxylating species.<sup>10, 20</sup> No turnover has ever been observed without the pterin cofactor bound.<sup>22</sup> The pterin cofactor is thought to be essential for producing the active hydroxylating species through proton-coupled electron transfer. The efforts of this study focus on characterizing the iron active site.

The known mechanistic data and overall reaction bear many similarities to cytochrome P450s (CYP450). The CYP450s contain cysteine-ligated hemes and hydroxylate their substrates via a two-electron oxidation.<sup>23-24</sup> Their mechanism also begins with substrate binding and is followed by reduction, dioxygen binding, and another reduction step leading to the formation of high-valent iron-oxo species which are very reactive and hydroxylate the nearby substrate.<sup>24</sup> Separate enzymes serve as reductases for CYP450s, but they too can hydroxylate substrate when supplied with an

external source of electrons.<sup>25</sup> Due to the similarities, the mechanism of NOS is postulated to be the same as CYP450s, at least for the first turnover.<sup>26</sup> The second turnover is unique in biology; there is no precedent for a three-electron oxidation of this sort.<sup>27</sup> It has been hypothesized that a protonated ferric-hydroperoxide may act as the nucleophile in the second turnover<sup>19</sup> rather than the ferryl-porphyrin radical cation known as Compound I.<sup>8</sup>



**Scheme 3.2.** The proposed catalytic cycle of nitric oxide synthase. Blue denotes species that have been proposed, but not observed. The numbers 1 and 2 in red show the pathway taken in each turnover.

Stopped-flow mixing coupled to UV-visible absorption spectroscopy is commonly used to observe catalytic intermediates. Unfortunately, the reactivity of nitric

oxide synthases is too fast to catch all of the intermediate steps. Using this technique, the final observable species before product formation is the ferrous-oxy (or ferric-superoxo depending on formal placement of the electron).<sup>6</sup> In the first turnover, the next species observed is the resting ferric state and in the second turnover it is the ferric-NO complex, which slowly releases NO to finish the cycle. No other intermediates can be seen by stopped-flow, presumably due to the speed with which they react.

Evidence supporting that the hydroperoxo species (in blue) is the active oxidant in the second turnover comes mainly from the ENDOR (electron-nuclear double resonance spectroscopy) studies conducted on the NOS from *Geobacillus stearothermophilus* (gsNOS) by Brian Hoffman and Roman Davydov.<sup>28-29</sup> These experiments show cleavage of the O-O bond prior to reaction with substrate in the first turnover, supporting the formation of Compound I or a similar species. In the second turnover, however, no cleavage of the O-O bond is observed prior to attack on substrate. They hypothesize that the presence of the hydroxyl group in NOHA makes the substrate easier to oxidize. The hydroperoxo heme complex might have enough oxidizing power to react with NOHA but not the arginine, requiring Compound I in the first turnover.

It is the O-O bond cleavage event that is vital to the reactivity of NOS and cyt. P450. Without this, Compound I cannot form and the active site will fail to produce a species with sufficient oxidizing power to react with substrates such as unactivated alkanes. It has been hypothesized that the role of the thiolate ligand is to promote this cleavage.<sup>30</sup> The strong  $\sigma$ -donating ability of the anionic ligand pushes more electron density into the iron and therefore also into the iron-oxygen bond and weakening the O-O bond. This has been dubbed the “thiolate push”.<sup>31</sup>

Upon closer inspection of the environment around the thiolate ligand, one finds a collection of three hydrogen bond (H-bond) donors all directed toward the thiolate. Comparison of gsNOS with other NOS enzymes reveals that these three hydrogen bond donors are universally conserved, with not a single exception.<sup>32</sup> This high level of conservation underscores their potential importance. Not only are they conserved in nitric oxide synthases, but the crystal structures of other heme thiolate enzymes reveal similarly conserved hydrogen bond donors in all. Cytochrome P450s (cyt. P450) all contain three H-bond donors; chloroperoxidase (CPO) contains only two such donors.<sup>3</sup>

When analyzing these polypeptide chains, one finds that in cyt. P450 and CPO all three donors in the proximal heme environment come not from amino acid side-chains but from amide protons in the backbone of the polypeptide chain. In NOS alone one and only one of the H-bond donors comes not from an amide but from the N-H of a tryptophan's indole ring, **Figure 3.1**. The universality of these H-bond donors pointing right at the axial thiolate ligand provokes questions of their function in the reactivity or stability or electronic tuning of these enzymes.

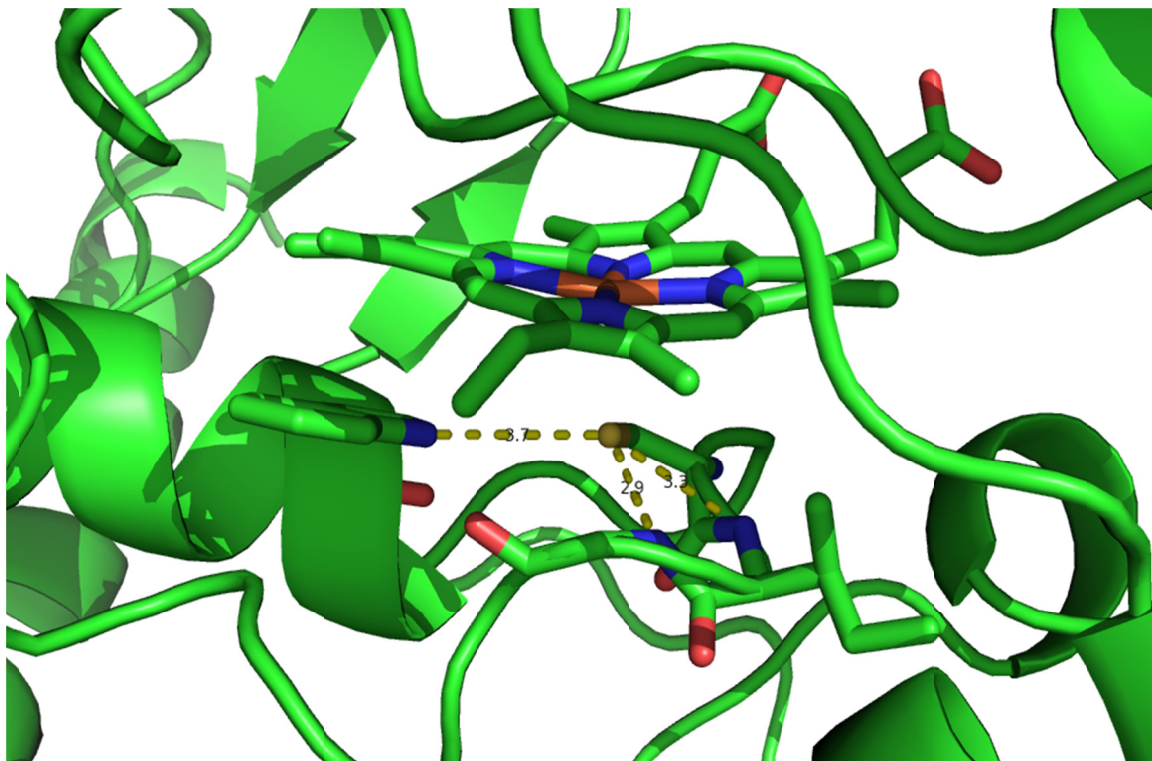


**Figure 3.1.** Close-up view of the heme center in a nitric oxide synthase showing the three hydrogen bond donors. The middle and the right are from amide groups on the protein backbone (2.9 and 3.3 Å) while the long H-bond on the left comes from a tryptophan residue at position 70 (very long at 3.7 Å) (PDB file 2FLQ).

Others have attempted to investigate the possible roles of these H-bond donors in cyt. P450.<sup>33-35</sup> The replacement of a glutamine that provides one amide group with a proline forces a kink in the loop below the heme and obviously replaces the N-H bond in the glutamine backbone with a N-C bond, incapable of participating in H-bonding. This also removes a hydrogen bond from the side chain of the Gln to the carbonyl moiety of the cysteine residue. The combination of these two effects as well as the shift in the backbone resulting from introduction of a proline makes results difficult to deconvolute. The work suggests, however, that this H-bond donor (not even a legitimate hydrogen bond) shifts the reduction potential of the heme by about +40 mV (removing it makes the potential more negative by about 40 mV).<sup>34</sup> Resonance Raman suggests that this H-bond

donor decreases the  $\sigma$ -donating ability of the thiolate significantly; its removal strengthens the iron-sulfur bond.<sup>33</sup> They “conclude that the functions of the proximal hydrogen bonding network in P450<sub>cam</sub> are to stabilize the heme-thiolate coordination, and to regulate the redox potential of the heme iron”.<sup>35</sup> While these conclusions seem reasonable, it is difficult to say the effect of a particular H-bond when several things are affected at once.

We wish to determine the role of these H-bond donors and support or refute the previous findings,<sup>36</sup> but particularly to study their effects in NOS. This family of enzymes provides a unique opportunity, given that one of the H-bond donors comes not from the backbone but from a side chain, allowing for facile and systematic variation using site-directed mutagenesis. Several such mutations have previously been made in NOS and characterized by resonance Raman.<sup>37-38</sup> These studies show that removal of this H-bond donor strengthens the Fe-S bond. No further characterization has been reported.

One other mutant of interest replaced the tryptophan with a histidine, preserving and possibly increasing the H-bond donating ability of the group. In this mutant, researchers actually saw a slower kinetics profile and possibly a new intermediate by stopped-flow spectroscopy.<sup>39</sup> No further characterization was reported, and this new intermediate was suggested to be Compound I, based solely upon the position of the Soret band (**Scheme 3.2**, the ferryl complex in blue). The lifetime of this new intermediate is on the order of a couple seconds before decaying to product. Compound I is formally a Fe(V) complex, with a ferryl and another radical cation sometimes found on the porphyrin ring. The likelihood of such a species living for that length of time is

incredibly low as it will be very reactive, making its assignment as Compound I doubtful.<sup>40</sup> No other investigations into the role of this H-bond donor have been made.

We investigated the role of these H-bond donors by systematically varying the functional groups on this side chain in question through the use of site-directed mutagenesis. The native tryptophan was replaced with histidine, phenylalanine, or tyrosine. Histidine can also participate in hydrogen bonding, but lacks the ability to  $\pi$ -stack with the porphyrin ring. Phenylalanine complements the histidine mutation in that it can  $\pi$ -stack but cannot hydrogen bond. The tyrosine can also  $\pi$ -stack, but the electronics should be significantly altered due to the presence of the hydroxyl group on the aryl ring, which is at an angle that should prohibit hydrogen bonding with the thiolate. These three mutants have been expressed and thoroughly characterized using the tools of modern bioinorganic chemistry to investigate the thermodynamics of the resulting active site (EPR, electrochemistry, etc.). These studies provide valuable insight into the specific role of these hydrogen bond donors and their purpose in NOS and other heme thiolate enzymes.

All studies were conducted using the nitric oxide synthase from the thermophilic bacterium *Geobacillus stearothermophilus*. This particular organism spends its entire existence at elevated temperatures, forcing the optimization of the function of its enzymes to this elevated temperature range (a thermal melting curve for the wild type enzyme gsNOS is shown in **Figure 3.2**). Due to this, the NOS from *G. bacillus* (gsNOS) functions optimally at temperatures well above other NOSs and shows a remarkably slowed kinetics profile at standard laboratory temperatures (such as 4 and 10 °C). Researchers conducted single turnover experiments with this enzyme and found it to form

a ferrous-oxy complex stable on the order of 60 seconds at 4 °C, which is remarkable. Thermophilic enzymes tend to be more stable under standard conditions in a research lab, unlike their mammalian counterparts which, in the case of NOS, often degrade in a matter of just a few hours at room temperature. This thermophilic enzyme provides a much more stable subject for the necessary detailed investigations and increases the likelihood of expressing appreciable yields of mutant forms in *E. coli*.

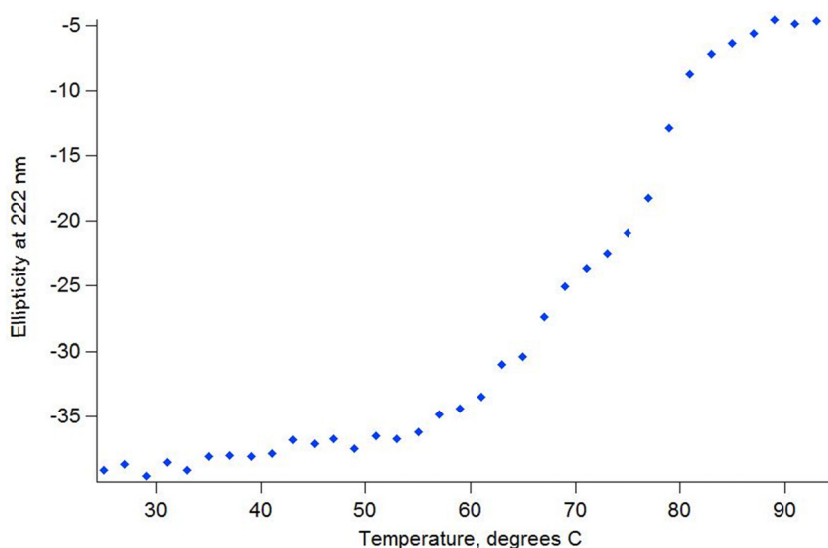


**Figure 3.2.** Thermal denaturation curve of wild type gsNOS as measured by circular dichroism spectroscopy. The midpoint of the melting curve is 74 °C.

This enzyme was first expressed and characterized in the lab of Brian Crane.<sup>41-42</sup>

Researchers were able to crystallize the enzyme and found the overall fold to be quite similar to that of other NOSs. Like bacterial enzymes, it lacks the zinc-binding domain which caps the pterin binding site. However, all other key structural features are preserved, including residues surrounding the substrate and cofactor binding sites and the dimer interface. The fold of the enzyme is slightly more compact than other NOSs (**Figure 3.3**), which may contribute to its thermal stability.

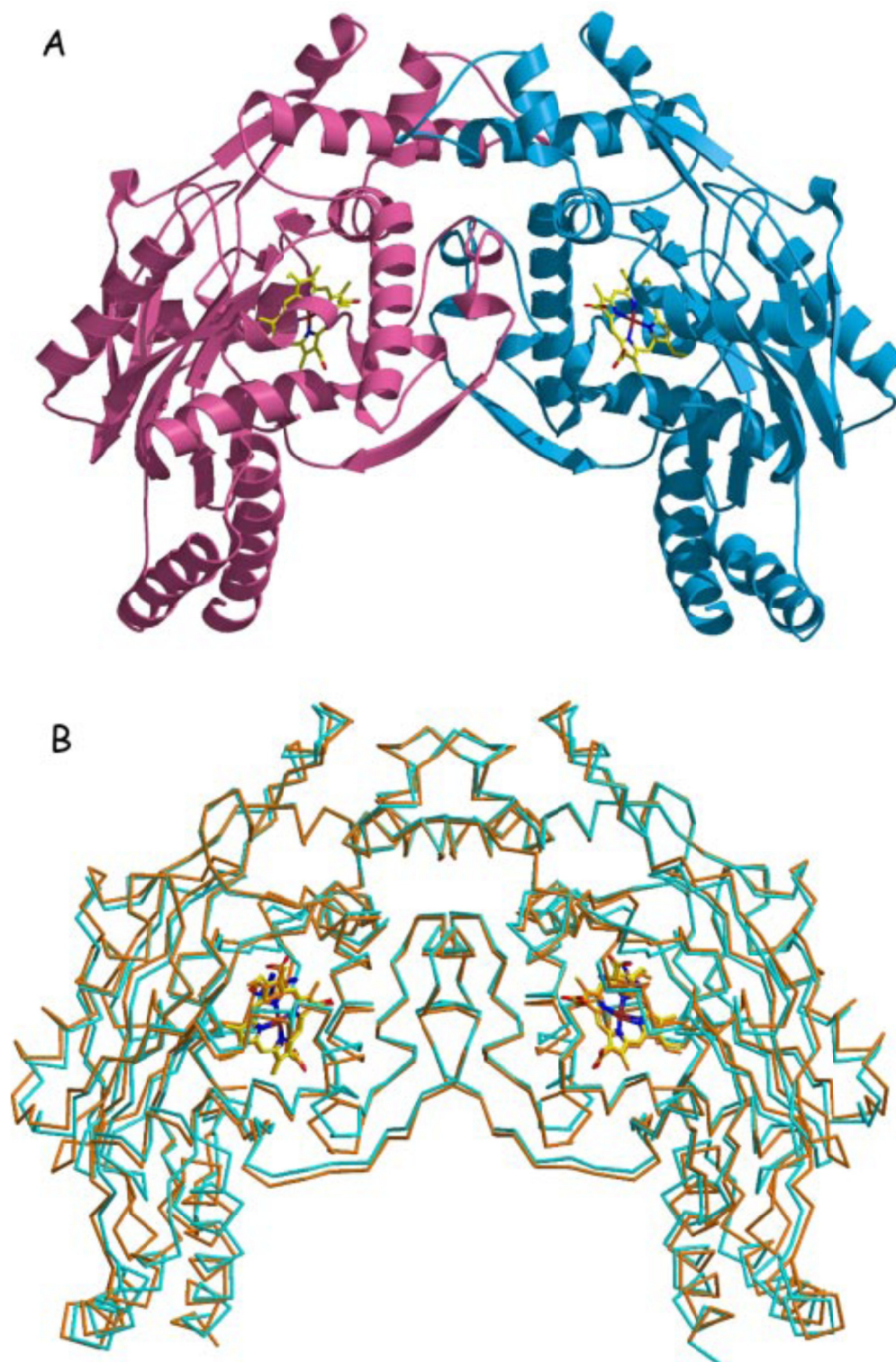


**Figure 3.3.** (A) The crystal structure of gsNOS showing the heme center. gsNOS crystallizes as a tight dimer, as is the case with all NOS enzymes. (B) Overlay of the backbones of gsNOS and NOS from *Bacillus subtilis* showing the increased packing and constriction in gsNOS.<sup>41</sup>

The wild type enzyme has a tryptophan residue at position 70 which hydrogen bonds with the thiolate ligand and  $\pi$ -stacks with the porphyrin ring of the heme. This Trp was replaced systematically by His, Tyr, and Phe. The wild type and these three mutant enzymes were studied by several techniques to characterize the thermodynamics of the active site. It was found that while these mutations do not greatly alter the stability of the protein or its overall fold, they do tune the electronics of the active site, shifting the spin state and altering the potential of the site.

### 3.3 Materials and Methods

#### *General*

The plasmid for the nitric oxide synthase from *Geobacillus stearothermophilus* was a gift from the lab of Brian Crane. This enzyme was expressed as previously described by Sudhamsu and Crane with no significant deviations in procedure.<sup>41</sup> The enzyme was overexpressed in *Escherichia coli* BL21 (DE3) cells. Cells were grown to an optical density of approximately 1.0–1.4 and induced by adding a solution containing iron(III) chloride, IPTG, and  $\delta$ -aminolevulinic acid (Aldrich) to final concentrations of 125 mg/L, 100  $\mu$ M, and 50 mg/L, respectively, in milliQ water. The pETDuet vector (Novagen) coded for a C-terminal cleavable His<sub>6</sub>-tag so samples were purified using metal affinity chromatography. (This vector also confers chloramphenicol resistance to the cells, so 34  $\mu$ g/mL of this antibiotic were added to all cultures in Luria broth.) The His<sub>6</sub>-tag was then cleaved using bovine thrombin (Calbiochem). Both thrombin and the His-tag were removed using size exclusion chromatography. Sample purity and Soret band epsilon values were determined through use of the Hemochromagen Assay.

A QuikChange site-directed mutagenesis kit from Stratagene was used to make the desired mutations in the amino acid chain. Primers were designed according to the guidelines outlined by the QuikChange kit manual. Unless otherwise noted, protein solutions were made in the following buffer: 50 mM Tris (2-amino-2-hydroxymethylpropane-1,3-diol), 150 mM NaCl, pH 7.5 (the same buffer used for size exclusion chromatography).

#### *Circular Dichroism Spectroscopy*

Circular dichroism spectroscopy was used to determine the stability of each protein sample. Chiral objects interact with circularly polarized light in such a way as to turn or distort the polarization of the light.<sup>43</sup> This is measured as ellipticity. Chiral features in macromolecules such as alpha helices or beta sheets are associated with particular signals by circular dichroism. Due to the size of the protein samples in question (gsNOS contains 375 residues with significant contributions from both alpha helices and beta sheets) the concentration of NOS in each cuvette was kept below 2  $\mu$ M. Samples with greater concentrations gave signals too large for the spectrometer to resolve. Alpha helices give characteristic ellipticity at 222 nm, to the red of the part of the spectrum where buffer would begin to affect the signal. For this reason, the standard Tris buffer was still used for these measurements. Spectra were collected scanning from 210 nm to 260 nm, stepping every one nm, to record the elliptical properties of the enzyme sample. In all cases the maximum signal was observed between 220 and 225 nm. To record the effects of temperature on each sample, the detector was fixed at 222 nm and the temperature was increased slowly, by steps of 2  $^{\circ}$ C, from 25 to 95  $^{\circ}$ C.

### *UV-Visible Absorption Spectroscopy*

UV-visible absorption spectroscopy is a particularly useful technique for characterizing heme proteins, as the position and shape of the Soret absorption band of the heme center is extremely sensitive to both the oxidation state of the iron and the coordination sphere around that iron. The maximum absorption of the Soret band can shift tens of Ångstroms due to simple additions of coordinating molecules such as imidazole or carbon monoxide.<sup>44</sup> UV-visible absorption spectra were acquired on an Agilent 8453 UV-visible spectrophotometer with a 2 nm resolution.

A common method for characterizing heme-thiolate enzymes and assessing their stability is by forming the ferrous-CO complex.<sup>37</sup> It is the strong, sharp absorption of this band at 450 nm that gives cytochrome P450 its name. The Soret band of ferrous-CO NOS typically lies to the blue of cyt. P450 at 446 nm. Samples were brought into an anaerobic glove box and reduced using dithionite. Excess dithionite was then removed using a PD-10 desalting column (although removal is not necessary in all situations). The samples are then sealed by Köntes valve in a quartz cuvette and brought out of the box. The headspace of this special cuvette was then connected to a tank of carbon monoxide and this gas was bubbled over the headspace, replacing the atmosphere. As CO diffuses into solution, the ferrous-CO complex is rapidly formed. The cuvette was then re-sealed and UV-vis spectra collected.

### *Hemochromagen Assay*

The heme center with its Soret absorption band provides a particularly useful handle for determining protein concentration as well. The Hemochromagen Assay allows researchers to characterize the molar absorptivities of heme centers in protein samples to

a degree that is far more accurate than the standard Bradford Assay.<sup>45</sup> In this method, the protein is denatured using strong base to liberate the heme center and pyridine is added in large excess to force coordination of the heme. This five-coordinate pyridine-heme is then reduced with dithionite to yield a ferrous complex (called a hemochrome) with a known and distinct absorption in the Q-band region. This new complex has two sharp Q-bands, the lower energy of which has a larger molar absorptivity of  $34,640 \text{ M}^{-1}\text{cm}^{-1}$ .<sup>45</sup> As long as the original spectrum of the fully-oxidized resting state of the enzyme is recorded first, the hemochrome can then be generated and the concentration of the sample can be calculated based on heme concentration using the known epsilon value of the hemochrome.

Samples of wild type gsNOS and all three mutants were made with absorbances between 0.3 and 1.0 (to keep the % transmittance within the best working range of the spectrophotometer). Each sample was prepared in a specialized cuvette (**Figure 3.4**), allowing the sealing of the sample from atmosphere, or its connection to a Schlenk line, all while in a quartz cuvette allowing for measurement of the UV-visible absorption spectrum. A spectrum of each protein sample was collected initially, before any additions or degassing; each sample was exactly 1 mL of approximately 4–10  $\mu\text{M}$  enzyme. Then 125  $\mu\text{L}$  of each pyridine and 1 M NaOH were added to the sample. The spectrum was again recorded to verify denaturation of the protein. Samples then had to be very thoroughly degassed through at least 30 rounds of gentle pump/purge to remove oxygen from the atmosphere and allow equilibration of the argon atmosphere with solution. Several crystals of solid dithionite were placed in the bulb, while the sample was kept anaerobic, and then the atmosphere above the dithionite was exchanged for argon again

on a Schlenk line. The spectrum of the degassed sample was recorded to determine any concentration changes due to the time spent under vacuum, and then the valve connecting the sample to the bulb containing dithionite was opened and the crystals of dithionite were added to reduce the system. This final spectrum was collected (quickly) and showed clearly the spectrum common to all hemochromes from systems with *b*-type hemes, two Q-bands, the redder of which has a larger epsilon and a maximum absorbance at 556 nm. This was used to determine the molar absorptivity of the heme center in each of the four protein samples studied.



**Figure 3.4.** Special cuvette used for Hemochromagen Assay, showing the bulb on the left and the quartz cuvette on the right.

### *Binding Assays*

The interaction of substrates with the active site can be characterized spectroscopically using UV-visible absorption spectroscopy. With heme proteins, the introduction of substrates or inhibitors to the binding pocket often shifts the position and shape of the Soret band in a characteristic manner.<sup>46</sup> Here, the substrate is arginine and the inhibitor is imidazole. The relationship between the concentration of substrate/inhibitor added and the resulting spectral shift has been calculated as follows in Equation 3.1,

$$\frac{1}{\Delta OD} = m \frac{1}{[imid]} - \frac{1}{K_S} \quad (3.1)$$

where  $\Delta OD$  is the change in absorbance due to the presence of the substrate or inhibitor and  $m$  is the slope of the resulting line,  $[imid]$  is the concentration of analyte added (in this case, imidazole).<sup>47</sup> This simple linear relationship allows for the calculation of a dissociation constant,  $K_S$ , through facile spectroscopic characterization by UV-vis (the symbol  $K_S$  is used to distinguish this term as a spectral dissociation constant rather than a traditional dissociation constant,  $K_D$ ). This technique requires a large shift in absorbance to give reliable results. In some cases, a competition assay was required in order to see significant shifts in the Soret band (the protein was pre-loaded with imidazole of a known concentration and then arginine was added to that sample to displace the imidazole).

### *Electron Paramagnetic Resonance Spectroscopy (EPR)*

One unique feature of heme-thiolate systems is related to the spin state of the iron. The electronics of these systems is poised just so that the pairing energy (the energetic cost of placing two electrons in the same orbital due to their mutual repulsion) and  $\Delta_{Octahedral}$  (the splitting between the  $E_g$  and  $T_{2g}$  states of the metal center) are nearly

identical. Under different conditions both high spin and low spin states can be observed, and often a mixture of the two states is seen. With Fe(III), high spin complexes have a spin of  $S = 5/2$  and low spin complexes have a spin of  $S = 1/2$ .

EPR requires the glassing of frozen samples and the random alignment of all paramagnetic species. In order to ensure glass formation, high glycerol concentrations are used. Samples were prepared with the following conditions: 20  $\mu\text{M}$  NOS, 20% by volume glycerol, 50 mM NaCl, 50 mM Tris at pH 7.5. Samples containing arginine had an Arg concentration of 300  $\mu\text{M}$  in order to ensure full formation of the arginine-bound complex, and all were pre-frozen by rapid immersion in liquid nitrogen. Spectra were collected using a Bruker EMX Biospin instrument with a Gunn diode microwave source. Liquid helium was used to cool the instrument and sample and spectra were collected at 20 K. EPR parameters were simulated using the software package SPINCOUNT.<sup>48</sup>

#### *Evans Method NMR*

To determine the spin state of samples at room temperature, Evans method nuclear magnetic resonance spectroscopy (NMR) was applied. With this method, one can determine the spin state of a sample by the paramagnet's affect on the surrounding solvent.<sup>49</sup> Samples were prepared with 1 mM protein sample inside of a capillary-like insert (Wilmad, part number WGS-5BL). These inserts are designed to fit inside of a standard NMR tube, with buffer in the surrounding space. This allowed the use of less than 100  $\mu\text{L}$  of protein sample, reducing the total amount of protein required. The presence of the paramagnetic iron center in the protein shifts the NMR peak of the water in the buffer. The magnitude of this shift is directly related to the concentration of the paramagnet and the number of unpaired electrons in that species (Equations 3.2, 3.3, and

3.4, specifically for a 600 MHz NMR spectrometer, from the manual for Chemistry 3b at Caltech). Samples were prepared with the standard buffer (50 mM Tris, 150 mM NaCl, pH 7.5) but with 20% D<sub>2</sub>O and 80% H<sub>2</sub>O rather than 100% H<sub>2</sub>O as an internal standard to allow for proper tuning of the magnet.

$$X_g = \left(\frac{3}{4\pi}\right) \left(\frac{\Delta\nu}{\nu}\right) \left(\frac{1}{m}\right) + X_0 \quad (3.2)$$

In the above equation,  $X_g$  is the gram susceptibility of the sample,  $\nu$  is the measured frequency of the NMR signal,  $m$  is the mass of the paramagnetic material in 1 mL of solution, and  $X_0$  is the gram susceptibility of the pure solvent (water being  $-7.203 \times 10^{-7} \text{ cm}^3 \text{ g}^{-1}$ ). This gram susceptibility is then used in Equation 3.3 to determine the number of unpaired electrons in the paramagnetic sample.

$$X_M = X_g M \quad (3.3)$$

$$\mu = 2.84\sqrt{X_M T} = \sqrt{n(n+2)} \quad (3.4)$$

$X_M$  is the molar susceptibility of the sample in question,  $M$  is its molecular weight, and  $T$  is the temperature in Kelvin. These equations allow one to calculate the number of unpaired electrons in a given system as long as the two solvent peaks (with and without the paramagnetic species) can be resolved.

### *Redox Titrations*

In order to measure the reduction potential of each protein sample, redox titrations were carried out. In this technique, a chemical oxidant or reductant is added to the protein sample. This chemical reactant should have a reduction potential close to that of the protein being studied ( $\pm 100 \text{ mV}$ ) in order to observe equilibrium between oxidized and reduced forms from sub-stoichiometric reaction with the protein sample. The reduction

potential of other NOSs has been measured previously and found to typically lie in the range of -250 to -300 mV vs. NHE.<sup>16, 39</sup>  $\text{Ru}^{3+}(\text{acac})_3$  was chosen as a chemical oxidant because it has a reversible reduction potential at -275 mV. The protein was reduced under inert atmosphere in a glove bag (experiments were carried out in the lab of Michael Marletta at UC Berkeley) and sealed in a cuvette along with the  $\text{Ru}(\text{acac})_3$  sample (in the syringe) of a specialized apparatus for this reaction shown in **Figure 3.5**. Small aliquots of ruthenium complex were added at a time, the sample was mixed and the resulting spectrum collected. This technique relies on the absorption of the oxidized and reduced species of one of the two reactants to be well resolved. From the UV-vis spectrum, the concentrations of the oxidized and reduced form of each of the two reactants can be calculated given the molar absorptivities and the Nernst Equation applied to give the reduction potential of the protein.

$$\Delta G = -nFE = -RT \ln K_{eq} \quad (3.5)$$

$$E = E^0 - \frac{RT}{nF} \ln K_{eq} \quad (3.6)$$



**Figure 3.5.** Apparatus for chemical redox titration. The protein sample is held in the quartz cuvette at the bottom, the oxidant/reductant is held in the gas-tight syringe above the cuvette. Samples can be degassed and assembled in an anaerobic chamber or degassed on a Schlenk line using the side arm (left).

### 3.4 Results and Discussion

#### *Enzyme Stability*

Circular dichroism spectroscopy was used to assess the stability of each of the protein samples studied. While only a single mutation was made, one residue can have a large effect on the overall fold of a macromolecule.<sup>50</sup> The tryptophan naturally occurring at this position in gsNOS is universally conserved in all nitric oxide synthases and it has been shown in cytochromes P450 that a phenylalanine residue at a similar location, which also  $\pi$ -stacks with the porphyrin ring is necessary for proper expression and folding of the enzyme.<sup>51</sup> This Trp not only  $\pi$ -stacks, but interacts with the axial thiolate through a long hydrogen bond. Removal of one or both of these functions could greatly affect the stability of the enzyme.

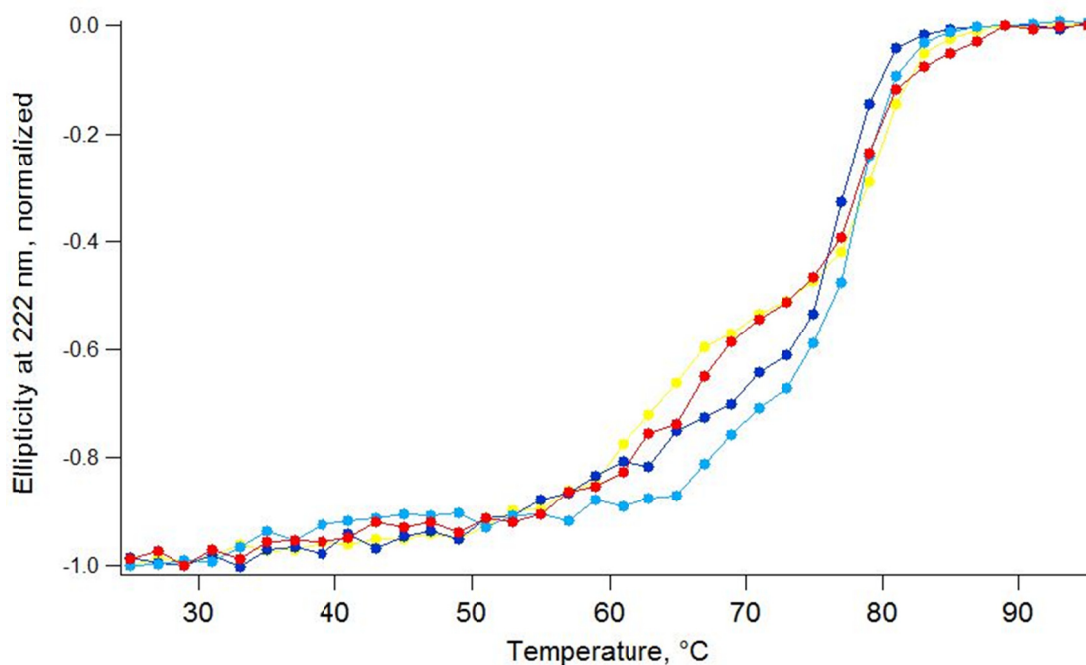


**Figure 3.6.** Thermal denaturation curves for each of the four protein samples studied herein, wild type (red), W70H (yellow), W70Y (light blue), and W70F (dark blue).

The thermal denaturation data collected show a somewhat remarkable result: none of the mutant enzymes shows a marked decrease in stability toward temperature. Given the two roles of this residue at position 70, it was hypothesized that these roles were vital to the fold of the protein. The fact that all four enzymes are stable to 60 °C and show similar behavior to the wild type above that temperature proves this hypothesis to be false. The His mutant (shown in yellow in **Figure 3.6**) may begin to unfold at slightly lower temperatures than wild type, consistent with the  $\pi$ -stacking of the Trp being important for positioning the heme in the enzyme. However, this effect is very small. The Tyr and Phe mutants, if anything, show increased stability over the wild type. Again, this is consistent with the hypothesis, as these two residues preserve the  $\pi$ -stacking function. They cannot provide a hydrogen bond to the thiolate (the hydroxyl group of the tyrosine side chain is pointed at an unfavorable angle, away from the thiolate), but the data show that this does not destabilize the enzyme.

Another common method for determining the stability of heme-thiolate enzymes involves the generation of the ferrous-CO complex. It is this form of the enzyme that absorbs strongly near 450 nm, giving cytochromes P450 their name. This tests specifically the stability of the heme center and the iron-thiolate bond. Cyt. P450s and NOSs are known to form an inactive form called P420 under some conditions.<sup>52</sup> This has been proposed to be either loss of axial thiolate coordination or protonation of the axial thiolate to make a neutral thiol ligand. In the case of NOS, it has even been shown to be reversible inactivation of the enzyme, but without the proper thiolate ligation the enzyme cannot produce NO.<sup>35, 52</sup>

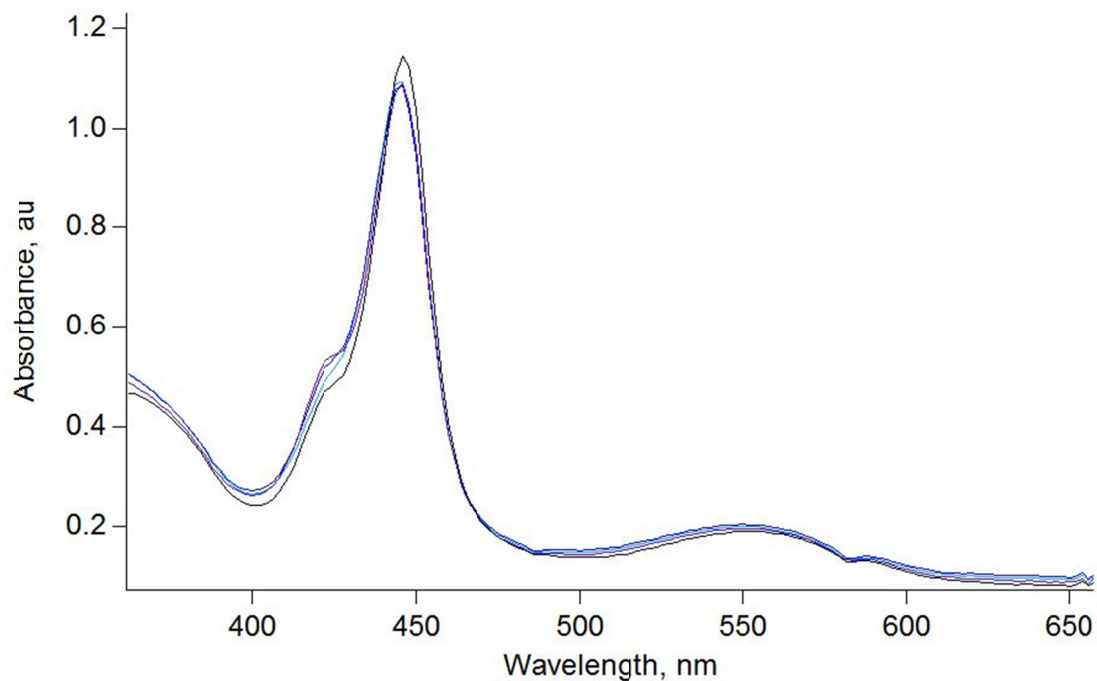


**Figure 3.7.** Ferrous-CO complex of wild type gsNOS, spectra collected over the course of 24 hours with no significant absorbance change.  $\lambda_{\text{max}} = 446$  nm.

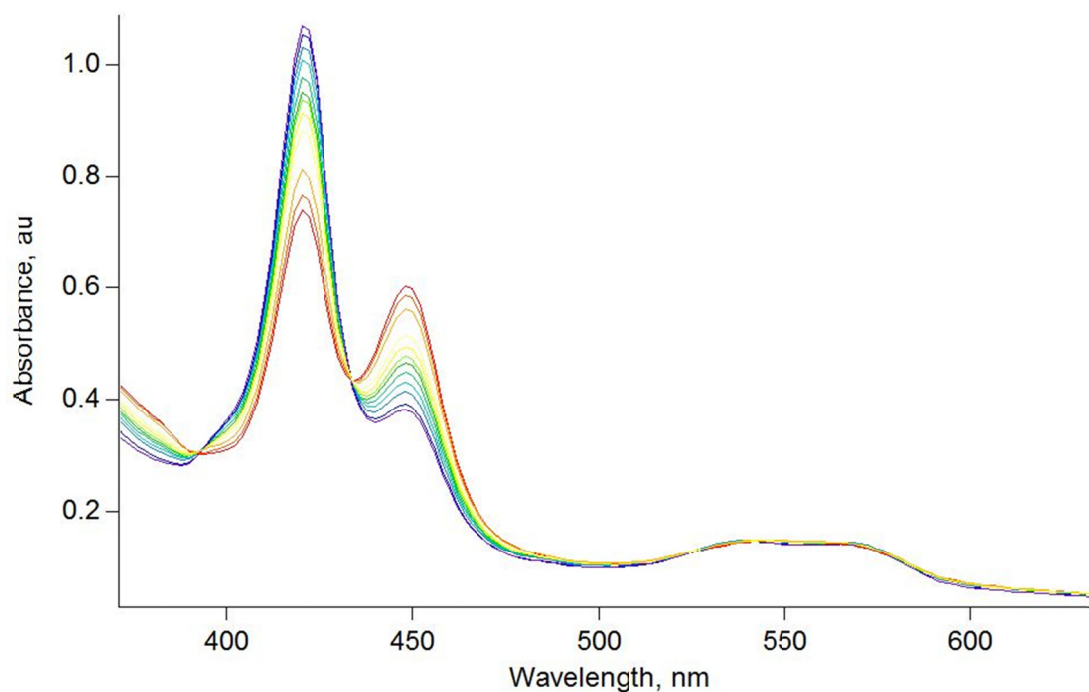


**Figure 3.8.** Ferrous-CO complex of W70F gsNOS, spectra collected over the course of 24 hours showing P420 formation, the first spectrum (red) was collected within 5 minutes of generating the complex.  $\lambda_{\text{max}} = 446$  nm decreasing, 420 nm increasing.

Upon formation of the ferrous-CO complex, the wild type gsNOS shows stable formation of the six-coordinate complex with maximum absorption at 446 nm as expected (**Figure 3.7**). The W70H mutant also shows stable formation of this complex, however with a blue-shifted Soret band at 440 nm. The reason for this blue shift is unknown, but may arise from altered tuning of the porphyrin ring. The two remaining mutant enzymes, W70Y and W70F, both remove hydrogen bonding capabilities. Over the course of 24 hours, both mutants show near complete formation of the P420 species (**Figure 3.8**). Removal of this one H-bond donor may increase interactions with the other two donors and increase the  $\sigma$ -donating ability of the thiolate ligand to the iron center. The data suggest that this third, distant (3.7 Å) H-bond donor stabilizes the enzyme in the active form by either decreasing the thiolate ligand's  $\sigma$ -donating ability or by preventing any one H-bond from being too strong in order to reduce the risk of protonation of the thiolate, or some combination thereof.

In the catalytic cycle of NOS, a similar ferrous-O<sub>2</sub> complex must form and remain stable on the timescale of catalysis in order for the enzyme to productively form NO. The electron density on the iron must be tuned in order to stabilize that six-coordinate species, yet still allow for ligand dissociation from the ferric-NO species formed in the last step of catalysis (**Scheme 3.2**). This unique requirement, the release of NO, may be the reason for the differences between the NOS and cyt. P450 proximal H-bonding network. In cyt. P450 all three H-bonds come from the amide backbone, while only two come from the backbone in NOS, the third coming from this Trp residue. Cyt. P450 has a separate phenylalanine residue for  $\pi$ -stacking with the porphyrin ring, rather than combining these two functions in a single Trp residue.<sup>38</sup>

### Binding Assays

Large changes in the UV-visible absorption of the heme center provide a clear handle for the study of ligand interactions with the active site. In nitric oxide synthases, the Soret band of the five-coordinate ferric complex (resting state of the enzyme) has a maximum absorbance at 396 nm. The six-coordinate complex, however, formed upon introduction of the inhibitor imidazole, has a sharp Soret band at 426 nm (**Figure 3.9**). These spectral changes can be used to calculate dissociation constants for inhibitors and substrates, as described in the Methods section using Equation 3.1.

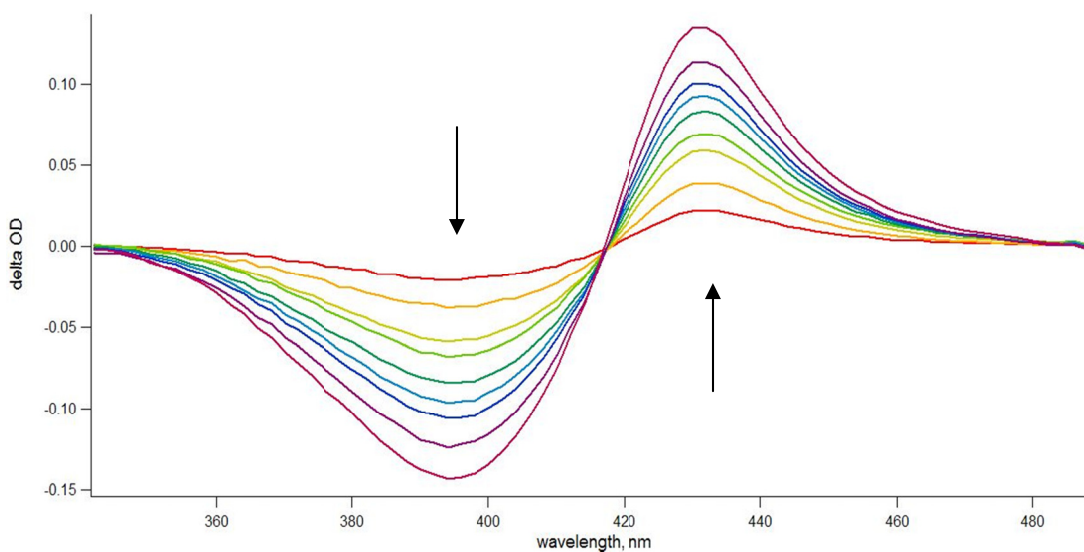


**Figure 3.9.** Spectral changes induced upon introduction of increasing concentrations of imidazole to wild type gsNOS.

According to Equation 3.1, plotting  $1/[\text{imidazole}]$  vs.  $1/\text{deltaOD}$  (x vs. y, the maximum absorbance change) should result in a linear relationship where  $m$  (the slope) depends on the concentration of protein in each sample, and the negative reciprocal of the y-intercept gives the spectral dissociation constant (**Figure 3.10**). The same can be done for the

substrate arginine, and each dissociation constant for arginine and imidazole from each of the four mutant enzymes is shown in **Table 3.1**.

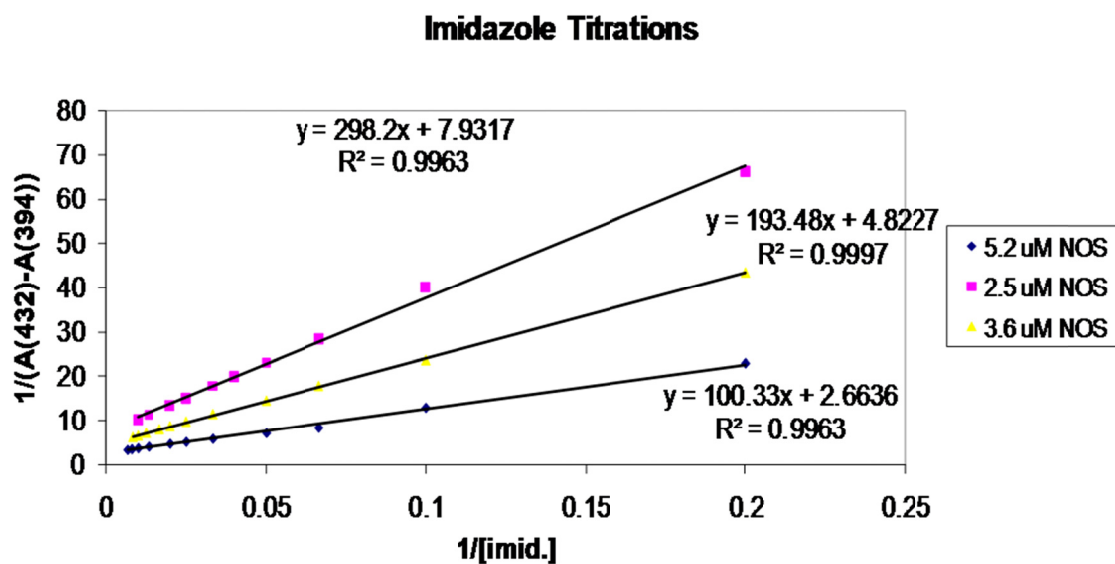


**Figure 3.10.** Calculation of the dissociation constant of imidazole from gsNOS.

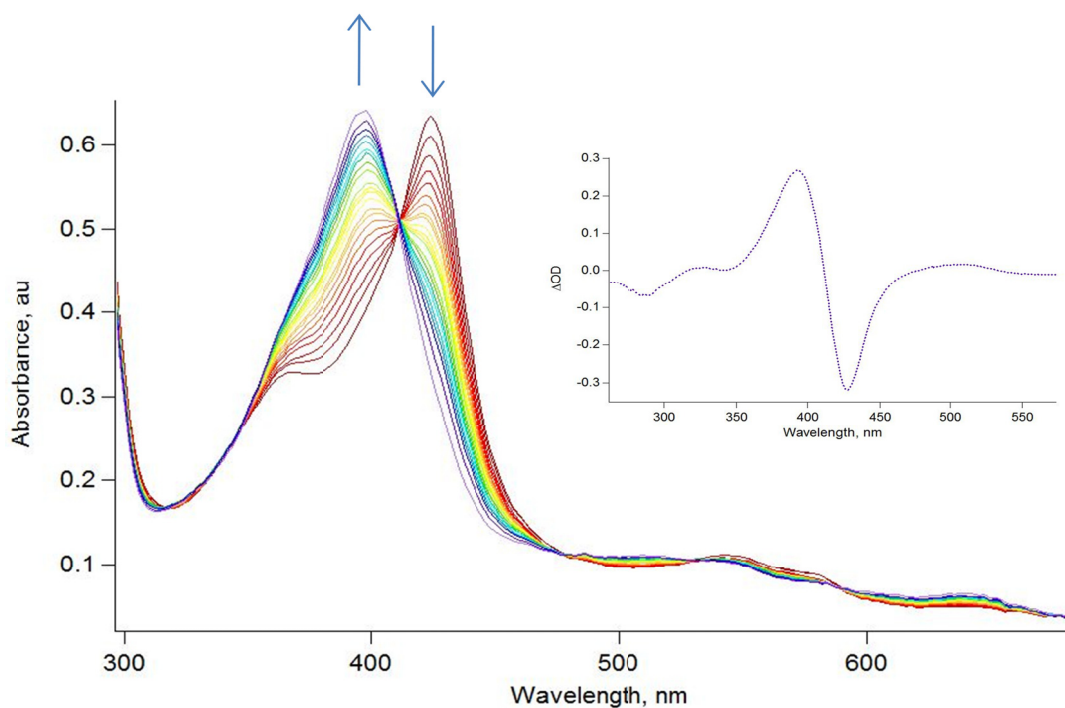


**Figure 3.11.** UV-visible absorbance changes upon introduction of arginine to a solution of wild type gsNOS with a known concentration of imidazole (20 mM) for a competitive binding assay.

**Table 3.1.** Spectral dissociation constants of imidazole and arginine.

( $\mu\text{M}$ )	$K_s$ (arg)	$K_s$ (imid)
WT	4.0	38
W70H	4.5	88
W70F	3.2	130
W70Y	4.3	210

It is clear from the values in **Table 3.1** that while the interaction of imidazole with the heme is greatly affected by mutations at position 70, the dissociation constant of arginine remains unaffected. This can be explained by the manner in which each substance binds. Arginine is positioned in the binding pocket above the heme, without directly ligating the iron. It is held in place by hydrogen bonds and hydrophobic contacts within the substrate channel.<sup>13, 53</sup> A high spin five-coordinate complex is formed; arginine merely kicks out the water molecule that weakly coordinates the iron. Imidazole, on the other hand, directly coordinates the iron, forming a bond between the iron and nitrogen of the ring. As the hydrogen bond donating group is removed, the thiolate becomes a better donor to the iron. This increases the electron density on the iron. The direct ligation of the imidazole forces even more electron density into the iron, which is disfavored, so as the thiolate becomes a better donor, the imidazole binds less tightly.

#### *UV-Visible Characterization of the Resting State*

As stated previously, electronic absorption spectroscopy is a useful tool for characterizing heme enzymes. The Hemochromagen Assay is used to determine protein concentration based on heme concentration. This assumes the presence of one heme unit per polypeptide chain. All measurements made herein depend on signal changes in the

spectra of the heme center (UV-vis, EPR, NMR due to the presence of paramagnetic iron center, etc.), thus any polypeptide chains of NOS that do not contain a heme unit will be invisible to all other measurements as well, making the Hemochromagen Assay the most appropriate measure of concentration for these purposes. The Bradford Assay is also commonly used to determine protein concentrations, but is less sensitive than the Hemochromagen Assay and detects all polypeptides including those without heme. Within the error of the experiment, all four proteins studied herein have similar Soret band molar absorptivities of about  $80,000 \text{ M}^{-1}\text{cm}^{-1}$ . The mutations appear not to greatly affect this value.

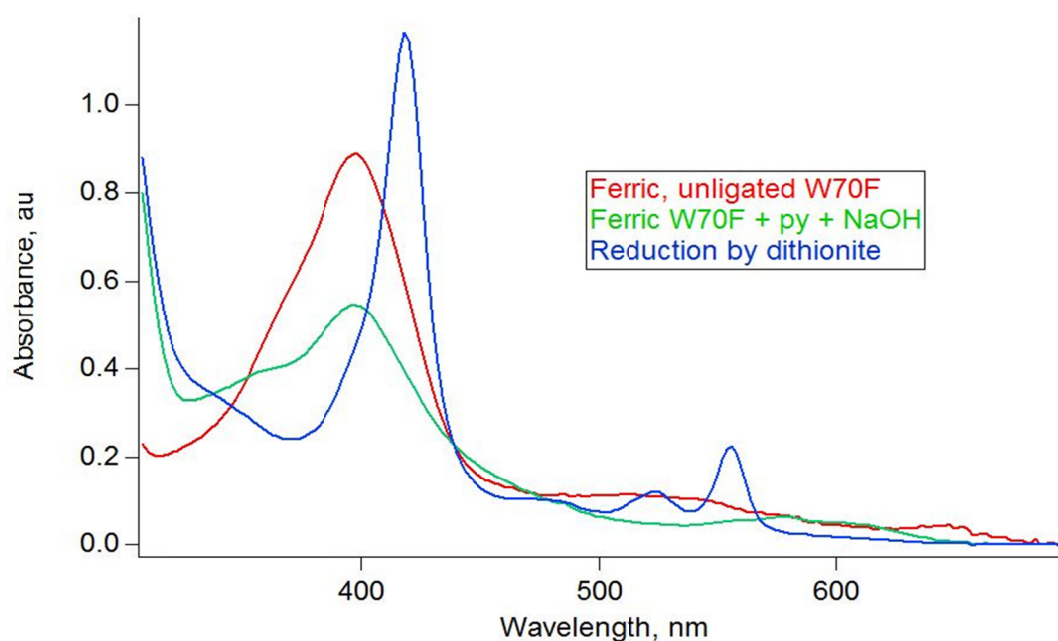
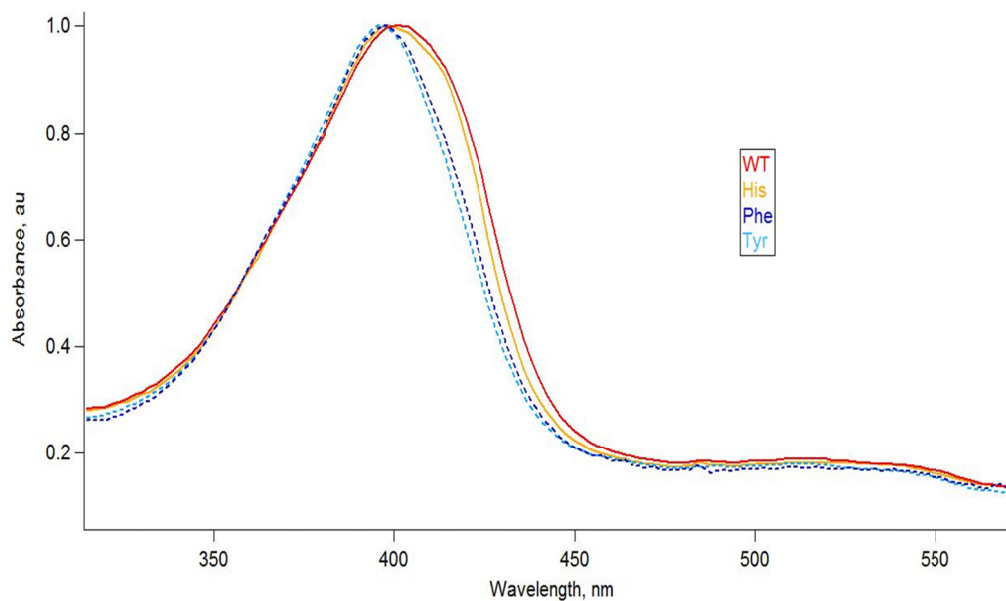


**Figure 3.12.** Formation of the five-coordinate Fe(II)(pyridine)(porphyrin) “hemochrome” complex with characteristic absorption bands in the Q-band region.

**Table 3.2.** Molar absorptivities of the four NOS mutants studied.

	Wild Type	W70H	W70F	W70Y
$\epsilon(\text{Soret}), \text{M}^{-1}\text{cm}^{-1}$	79,000	73,000	84,000	78,000

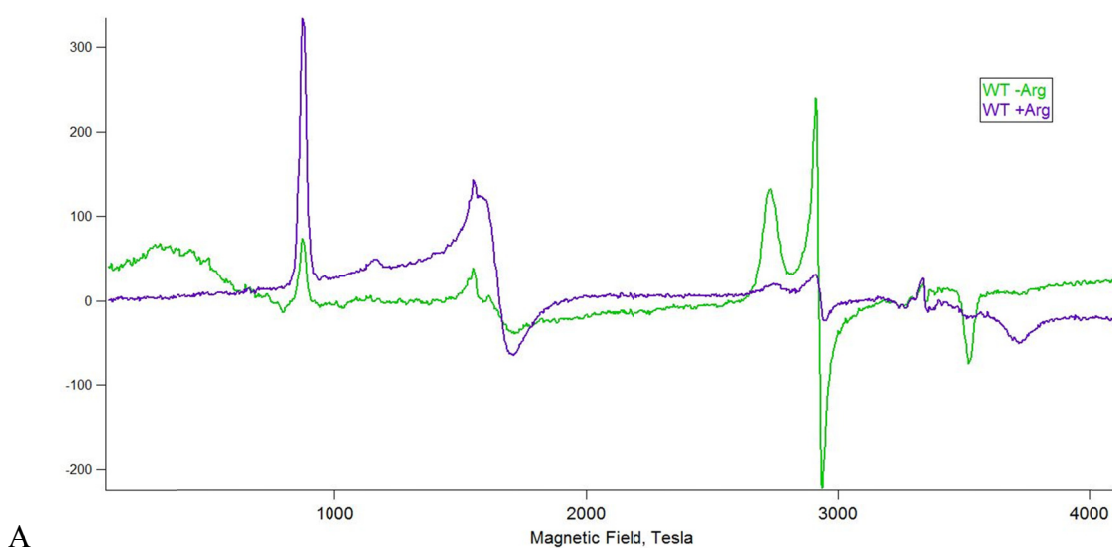
It was observed, however, that mutations at position 70 affect the shape of the Soret band. As seen in **Figure 3.13**, removal of the hydrogen-bond donating group by introduction of a Phe or a Tyr leads to sharpening of the Soret band, while the His mutant preserves both the H-bond and the broader shape of the peak. It is known that displacing the loosely coordinated water molecule in the distal axial position converts the iron center from a mixture of spin states to the high-spin five-coordinate complex.<sup>54</sup> Other cyt. P450s has Soret bands further to the red in the resting state without substrate (P450cam has a maximum at 417 and P450-BM3 at 418 nm)<sup>55</sup> that shift to approximately 400 nm upon introduction of substrate (camphor or a long chain fatty acid). This observed shift in Soret band location and shape in **Figure 3.13** may arise from the shifting of the iron center further towards high spin. The UV-vis spectra suggest that the two mutants without an H-bond donor at position 70 have almost no water coordination (the equilibrium lies far to the five-coordinate state) due to the increased donating abilities of the thiolate ligand.



**Figure 3.13.** Absorption spectra in the visible region of all four protein samples under investigation. Wild type (red), W70H (yellow), W70F (dark blue), W70Y (light blue).

### *Characterization of the Resting Spin State*

In order to investigate the spin state of each of these samples, electron paramagnetic resonance spectroscopy was employed. Experiments were carried out at 20 K with and without arginine, as this should force complete formation of the high spin complex. Unfortunately, in all cases signals could be observed for both the low and high spin complex, even after addition of the substrate. By EPR the samples appear predominantly low spin in the absence of substrate, arginine inducing a near complete shift to high spin (**Figure 3.14**). UV-visible spectroscopy suggests that all samples are composed of mostly the high spin complex, based on the position of the Soret band. All signals are similar to the reported values for mammalian NOSs (**Table 3.3**).<sup>56-57</sup>



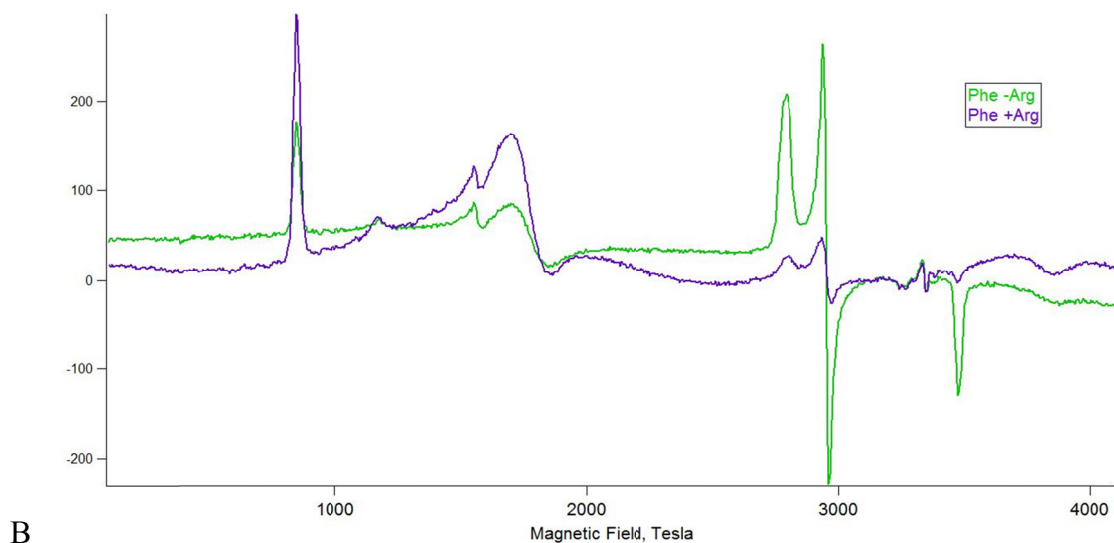


**Figure 3.14.** (A) EPR spectra of wild type gsNOS (representative of the His mutant as well) with (purple) and without (green) the substrate arginine. (B) EPR spectra of the W70F mutant of gsNOS (representative of the W70Y mutant as well) with (purple) and without (green) the substrate arginine.

**Table 3.3.** EPR parameters for both high and low spin states of the heme center.

	Spin State	$g(x)$	$g(y)$	$g(z)$
w.t.	high	7.69	4.10	1.80
His	high	7.69	4.12	1.81
Phe	high	7.95	3.78	1.73
Tyr	high	7.88	3.89	1.76
<b>w.t.</b>	<b>low</b>	<b>1.90</b>	<b>2.29</b>	<b>2.46</b>
<b>His</b>	<b>low</b>	<b>1.90</b>	<b>2.29</b>	<b>2.47</b>
<b>Phe</b>	<b>low</b>	<b>1.93</b>	<b>2.27</b>	<b>2.40</b>
<b>Tyr</b>	<b>low</b>	<b>1.92</b>	<b>2.28</b>	<b>2.41</b>

It was hypothesized that the large temperature difference could be the cause of this discrepancy. Evans method is an NMR-based technique for the determination of

paramagnetic spin state. NMR experiments can be carried out at room temperature, allowing for a more direct comparison with UV-vis. The presence of paramagnetic compounds in high concentrations shifts the resonance of the solvent peak. This shift is related to the number of unpaired electrons in the complex by the Equations 3.2, 3.3, and 3.4. **Table 3.4** shows results of these measurements. Strengthening the H-bonding capabilities of the residue at position 70 decreases the number of unpaired electrons relative to wild type, while removing that H-bond increases the number of unpaired electrons and shifts the sample further towards high spin. These results agree with those from UV-vis and together confirm that the enzyme is predominantly high spin in character at room temperature (low spin would have one unpaired electron, high spin would have five).

**Table 3.4.** Unpaired electrons for each mutant as determined by Evans method.

Sample	delta, ppm	[NOS], mM	n (unpaired e)
WT	0.041	1.00	3.9
His	0.040	1.26	3.3
Phe	0.057	1.16	4.4
Tyr	0.062	1.38	4.1

### *Redox Titrations*

In order to fully characterize the electronics of the ground state of each enzyme's active site, a measurement of the heme ( $\text{Fe}^{3+/2+}$ ) reduction potential is necessary. Determination of the reduction potential of a redox active center is not always straightforward, particularly when the complex of interest is buried within a protein

scaffold. The backbone of a protein is made mostly from insulating C-C and C-N bonds and is designed to discourage random electron transfer reactions in favor of one particular function of the enzyme. Nature must find the balance between discouraging deleterious redox reactions and promoting productive reactions. The presence of the protein scaffold buries the active site and in most cases prevents communication with electrodes, rendering standard electrochemical techniques useless. Small molecules, however, which can freely diffuse through solution, can still react with most metal sites within proteins. For this reason, chemical redox titrations are the method of choice for measuring reduction potentials.

For chemical redox titrations no electrodes or potentiostats are required; however, spectroscopic handles are necessary to indicate that a redox process has occurred. Many metalloproteins have absorption bands in the visible region, making them amenable to characterization by UV-visible spectroscopy. Provided there are wavelengths where the two redox forms show characteristic absorption bands, relative protein concentration can be measured. A chemical oxidant/reductant is employed with a known reduction potential near (within  $\pm 100$  mV) the expected potential of the protein under analysis, in this case Ru(acac)<sub>3</sub> with a Ru<sup>3+/2+</sup> reduction potential of -275 mV vs. NHE. This feature is required for the measurement of a precise equilibrium constant in Equation 3.6 as sub-stoichiometric reactions will be observed. A small molecule chemical titrant must be designed to have desirable UV-visible absorption properties so as not to obscure the changes taking place with the enzyme as well as a potential close to that of the sample in order to observe equilibrium between the two. However, if the titrant has clear optical changes upon change in oxidation state, it too can be used to calculate the concentration

of each species in solution. Equation 3.6 is employed, where  $E$  is the difference between the reduction potential of the titrant and the protein, and  $E^0$  is the reduction potential of the titrant itself.

First, the optical spectra of Ru(acac)<sub>3</sub> were recorded at various potentials using a standard spectroelectrochemical cell (CH Instruments) (**Figure 3.15**). A solution of 95 μM Ru(acac)<sub>3</sub> in 150 mM NaCl, 50 mM Tris, pH 7.5 was made and degassed to remove oxygen from solution. The potential was held at -400 mV vs. the Ag/AgCl reference electrode (about -200 vs. NHE) for a few minutes to allow full equilibration and the first spectrum (in red) was recorded. The potential was then stepped in 20 mV increments (10 mV when nearing the reduction potential of the compound) to the negative, each time several minutes were allowed for full equilibration of the solution before a UV-vis spectrum was recorded. This was continued until no further optical changes were detected (the final spectrum is shown in purple). These data confirm the reported reduction potential of -275mV and identify isosbestic points at 290 and 398 nm.

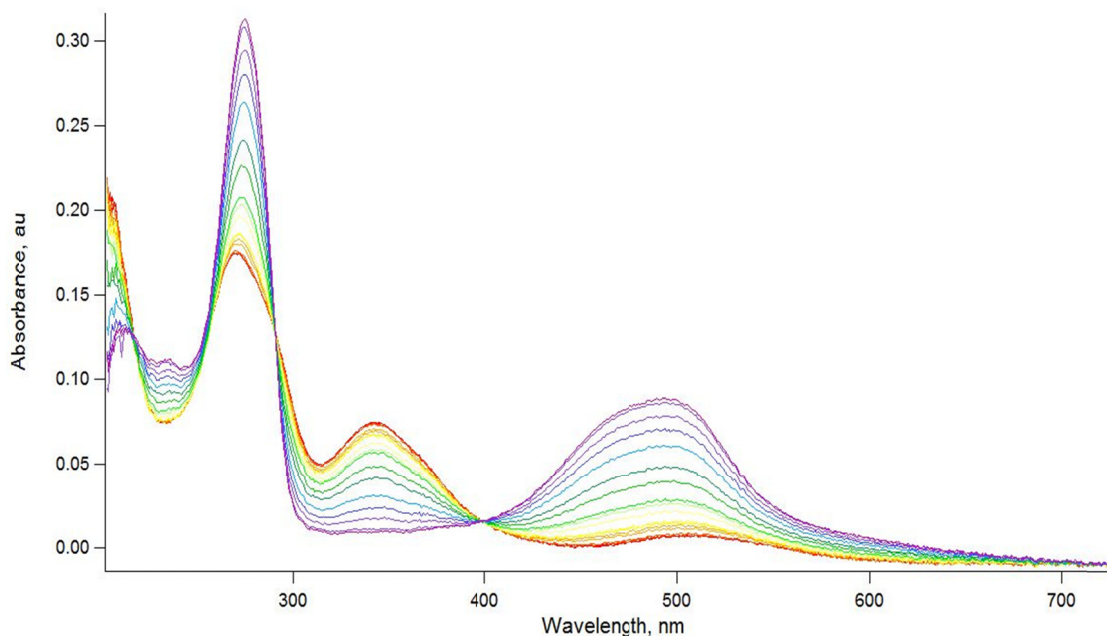


**Figure 3.15.** Spectroelectrochemical characterization of Ru(acac)<sub>3</sub>, 95  $\mu$ M in Tris buffer. Oxidized, Ru(III), red. Reduced, Ru(II), purple.

This ruthenium complex was then used to oxidize the reduced form of each enzyme. Samples of five-coordinate ferrous enzyme were made in an anaerobic chamber and excess reductant was removed using desalting columns. The sample was then sealed in a specialized cuvette (**Figure 3.5**) with Ru(III)(acac)<sub>3</sub> in the syringe. This ruthenium complex was then added in a stepwise manner and UV-vis spectra were recorded along the way (**Figures 3.16 and 3.17**). These measurements are extremely sensitive to the presence of any oxygen, as it reacts rapidly and stoichiometrically with the reduced iron center. Any leak would cause large deviations in observed spectra.

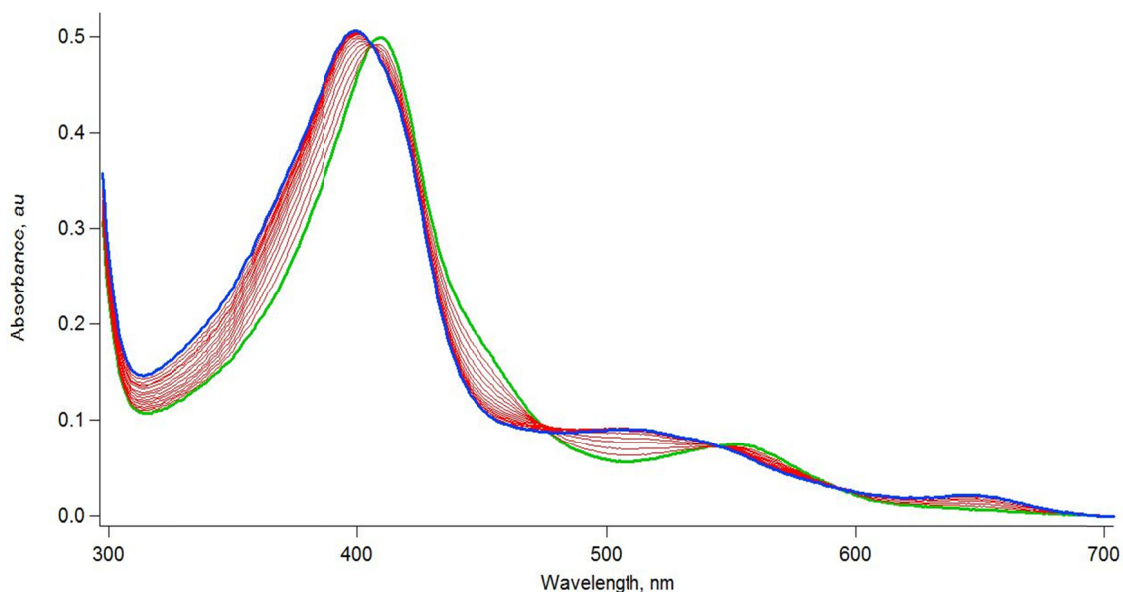


**Figure 3.16.** Redox titration using  $\text{Ru}(\text{acac})_3$  to oxidize wild type ferrous gsNOS, showing a shift from reduced NOS (green) to oxidized protein plus excess Ru complex (blue).

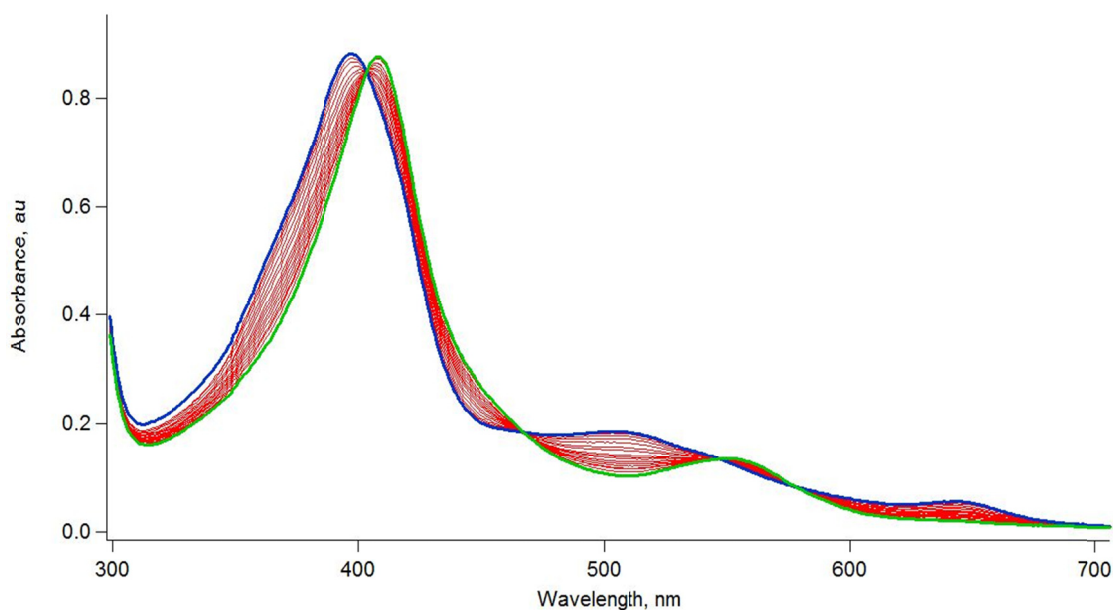


**Figure 3.17.** Titration using  $\text{Ru}(\text{acac})_3$  to oxidize W70F ferrous gsNOS, showing a shift from reduced NOS (green) to oxidized protein plus excess Ru complex (blue).

Accurate measurement of reduction potentials is particularly difficult when the potentials in question are very negative of 0 vs. NHE and reactions are slow, as is the

case here. Reliable potentials were determined for wild type ( $-362 \pm 5$  mV) and W70H ( $-339 \pm 5$  mV). These numbers are both within 100 mV of the potential of the chemical titrant,  $\text{Ru}(\text{acac})_3$ . The other two mutant enzymes, however, should have significantly lower potentials as the thiolate ligand becomes a better donor to the iron as literature suggests.<sup>38</sup> This would lead to stoichiometric reaction with the Ru complex. If equilibrium cannot be observed, the potential of the iron site cannot be determined. This was in fact the case, as only stoichiometric oxidation of the iron was observed and no measure of the  $K_{\text{eq}}$  could be obtained for W70F and W70Y. It is sufficient to conclude that removal of this strategic hydrogen bond donor substantially decreases the reduction potential of the center, consistent with the lack of stability in the ferrous-CO complexes of these two mutants.

It is also of note that the potentials measured for wild type and W70H are not as expected from previous work.<sup>58</sup> The potential of most NOS enzymes falls between -240 and -270 mV vs. NHE. One exception to this is mammalian inducible NOS which has a potential near -350 mV without substrate present.<sup>16</sup> This is too negative to be reduced by the flavins in the NOS reductase domain. Upon introduction of the substrate, the potential shifts up toward -250 mV and the iron center can now be reduced by the flavins. In other mammalian forms, the presence of calcium ions regulates electron transfer between the two domains. In its absence, the oxygenase domain and reductase domain are too far separated for electron transfer to occur. In inducible NOS, the activity of which is independent of calcium ion concentration, it is this redox switch that most likely prevents deleterious side reactions. (If the heme center is reduced without substrate present, reactive oxygen species are formed which can damage the cell. However, if the heme is

only reduced when the substrate is present, this unproductive reduction event is avoided.) This is the first measurement of the reduction potential of any bacterial NOS. These enzymes may be regulated in a manner similar to inducible NOS, which is fitting in light of their lack of dedicated reductase domain.

The potential of the histidine-containing mutant lies positive of the wild type enzyme. This same effect was seen in inducible NOS, where the corresponding mutation (W188H) shifts the potential positive by 88 mV (as opposed to only 20 mV as seen here). It may be that the tighter fold of gsNOS alters this interaction relative to inducible NOS. The histidine may not come into as close contact as the tryptophan, or the electronics of the porphyrin ring may be affected in a unique way. A crystal structure of these mutant enzymes would aid in this discussion. Samples have been sent to the lab of Brian Crane at Cornell, however crystals of NOS are notoriously difficult and slow-growing. Efforts to determine the structure of these three new mutants are ongoing.

### **3.5 Conclusions**

The thermodynamics of wild type and three mutants of gsNOS were characterized by various methods. Data from circular dichroism spectroscopy show that mutations at position 70 do not decrease the overall stability of the protein fold. The evidence from multiple techniques is clear, however, that these mutations significantly affect the electronics of the heme center. It was shown using binding assays, generation of the ferrous-CO species, and redox titrations that the  $\sigma$ -donating abilities of the thiolate are increased after removal of the hydrogen bonding group in the Trp. Both chemical redox titrations and instability of ferrous-CO complexes of the two mutants lacking this key

hydrogen bond (W70F and W70Y) suggest that they have more negative reduction potentials than the two mutants with this hydrogen bond (wild type and W70H). Evans used NMR to confirm the results of UV-visible spectroscopy which suggest that removal of this hydrogen bond shifts the heme center toward the high-spin state due to strengthening of the Fe-S bond, as seen in the binding assays.

It can be concluded that this universally-conserved tryptophan residue serves several roles, but positioning of the heme within the protein (as has been suggested for cyt. P450s) is not one of them. In order to produce NO the electronics of the heme center must be tuned in such a way as to stabilize high-valent iron species for the oxidation of substrate. During catalysis, the site must also be tuned not only to support six-coordinate ferrous-oxy complex, but promote release of NO $\cdot$  from the heme in the end. If the  $3/2+$  reduction potential of the site is too negative, the ferrous-oxy may be unstable or the high-valent iron species too stable to perform the desired reactivity. If too negative, release of NO will be disfavored and decrease the rate of release to undesirable levels. The reactivity of these mutants will shed further light on the role of this key hydrogen-bond donating group.

### 3.6 References

1. Denisov, I. G., Makris, T. M., Sligar, S. G., and Schlichting, I. (2005) Structure and chemistry of cytochrome p450, *Chem. Rev.* 105, 2253.
2. Alderton, W. K., Cooper, C. E., and Knowles, R. G. (2001) Nitric oxide synthases: Structure, function and inhibition, *Biochem. J.* 357, 593.
3. Sono, M., Roach, M. P., Coulter, E. D., and Dawson, J. H. (1996) Heme-containing oxygenases, *Chem. Rev.* 96, 2841.
4. Dawson, J. H., and Sono, M. (1987) Cytochrome.P-450 and chloroperoxidase - thiolate-ligated heme enzymes - spectroscopic determination of their active-site structures and mechanistic implications of thiolate ligation, *Chem. Rev.* 87, 1255.
5. Li, H. Y., Igarashi, J., Jamal, J., Yang, W. P., and Poulos, T. L. (2006) Structural studies of constitutive nitric oxide synthases with diatomic ligands bound, *J. Biol. Inorg. Chem.* 11, 753.
6. Stuehr, D. J., Santolini, J., Wang, Z. Q., Wei, C. C., and Adak, S. (2004) Update on mechanism and catalytic regulation in the no synthases, *J. Biol. Chem.* 279, 36167.
7. Marletta, M. A. (1993) Nitric oxide synthase structure and mechanism, *J. Biol. Chem.* 268, 12231.
8. Alderton, W. K., Cooper, C. E., and Knowles, R. G. (2001) Nitric oxide synthases: Structure, function and inhibition, *Biochem. J.* 357, 593.
9. Stuehr, D. J., Cho, H. J., Kwon, N. S., Weise, M. F., and Nathan, C. F. (1991) Purification and characterization of the cytokine-induced macrophage nitric-oxide synthase - an fad-containing and fmn-containing flavoprotein, *Proc. Nat. Acad. Sci. USA* 88, 7773.
10. Hurshman, A. R., and Marletta, M. A. (2002) Reactions catalyzed by the heme domain of inducible nitric oxide synthase: Evidence for the involvement of tetrahydrobiopterin in electron transfer, *Biochemistry* 41, 3439.
11. Hevel, J. M., and Marletta, M. A. (1992) Macrophage nitric-oxide synthase - relationship between enzyme-bound tetrahydrobiopterin and synthase activity, *Biochemistry* 31, 7160.
12. Hurshman, A. R., Krebs, C., Edmondson, D. E., Huynh, B. H., and Marletta, M. A. (1999) Formation of a pterin radical in the reaction of the heme domain of inducible nitric oxide synthase with oxygen, *Biochemistry* 38, 15689.
13. Crane, B. R., Arvai, A. S., Ghosh, D. K., Wu, C. Q., Getzoff, E. D., Stuehr, D. J., and Tainer, J. A. (1998) Structure of nitric oxide synthase oxygenase dimer with pterin and substrate, *Science* 279, 2121.
14. Garcin, E. D., Bruns, C. M., Lloyd, S. J., Hosfield, D., Tiso, M., Stuehr, D. J., Tainer, J. A., and Getzoff, E. D. (2004) Structural basis for isozyme specific regulation of electron transfer in nitric oxide synthase, *J. Biol. Chem.* 279, 37918.
15. Zhu, Y., and Silverman, R. B. (2008) Revisiting heme mechanisms. A perspective on the mechanisms of nitric oxide synthase (nos), heme oxygenase (ho), and cytochrome p450s (cyp450s), *Biochemistry*.
16. Presta, A., Weber-Main, A. M., Stankovich, M. T., and Stuehr, D. J. (1998) Comparative effects of substrates and pterin cofactor on the heme midpoint

- potential in inducible and neuronal nitric oxide synthases, *J. Am. Chem. Soc.* *120*, 9460.
17. Lippard, S. J., Berg, J. M. (1994) *Principles of bioinorganic chemistry*, University Science Books, Mill Valley, CA.
  18. Hurshman, A. R., and Marletta, M. A. (1995) Nitric oxide complexes of inducible nitric oxide synthase: Spectral characterization and effect on catalytic activity, *Biochemistry* *34*, 5627.
  19. Belliston-Bittner, W., Dunn, A. R., Nguyen, Y. H. L., Stuehr, D. J., Winkler, J. R., and Gray, H. B. (2005) Picosecond photoreduction of inducible nitric oxide synthase by rhenium(i)-diimine wires, *J. Am. Chem. Soc.* *127*, 15907.
  20. Wang, Z. Q., Wei, C. C., Santolini, J., Panda, K., Wang, Q., and Stuehr, D. J. (2005) A tryptophan that modulates tetrahydrobiopterin-dependent electron transfer in nitric oxide synthase regulates enzyme catalysis by additional mechanisms, *Biochemistry* *44*, 4676.
  21. Wei, C. C., Wang, Z. Q., Hemann, C., Hille, R., and Stuehr, D. J. (2003) A tetrahydrobiopterin radical forms and then becomes reduced during n-omega-hydroxyarginine oxidation by nitric-oxide synthase, *J. Biol. Chem.* *278*, 46668.
  22. Ghosh, D. K., Wu, C. Q., Pitters, E., Moloney, M., Werner, E. R., Mayer, B., and Stuehr, D. J. (1997) Characterization of the inducible nitric oxide synthase oxygenase domain identifies a 49 amino acid segment required for subunit dimerization and tetrahydrobiopterin interaction, *Biochemistry* *36*, 10609.
  23. Denisov, I. G., Makris, T. M., Sligar, S. G., and Schlichting, I. (2005) Structure and chemistry of cytochrome p450, *Chem. Rev.* *105*, 2253.
  24. Meunier, B., de Visser, S. P., and Shaik, S. (2004) Mechanism of oxidation reactions catalyzed by cytochrome p450 enzymes, *Chem. Rev.* *104*, 3947.
  25. Udit, A. K., Hill, M. G., and Gray, H. B. (2006) Electrochemistry of cytochrome p450<sub>bm3</sub> in sodium dodecyl sulfate films, *Langmuir* *22*, 10854.
  26. Udit, A. K., Belliston-Bittner, W., Glazer, E. C., Le Nguyen, Y. H., Gillan, J. M., Hill, M. G., Marletta, M. A., Goodin, D. B., and Gray, H. B. (2005) Redox couples of inducible nitric oxide synthase, *J. Am. Chem. Soc.* *127*, 11212.
  27. Martin, N. I., Woodward, J. J., Winter, M. B., Beeson, W. T., and Marletta, M. A. (2007) Design and synthesis of c5 methylated l-arginine analogues as active site probes for nitric oxide synthase, *J. Am. Chem. Soc.* *129*, 12563.
  28. Davydov, R., Sudhamsu, J., Lees, N. S., Crane, B. R., and Hoffman, B. M. (2009) Epr and endor characterization of the reactive intermediates in the generation of no by cryoreduced oxy-nitric oxide synthase from geobacillus stearothermophilus, *J. Am. Chem. Soc.* *131*, 14493.
  29. Davydov, R., Ledbetter-Rogers, A., Martásek, P., Larukhin, M., Sono, M., Dawson, J. H., Masters, B. S. S., and Hoffman, B. M. (2002) Epr and endor characterization of intermediates in the cryoreduced oxy-nitric oxide synthase heme domain with bound l-arginine or n<sup>g</sup>-hydroxyarginine, *Biochemistry* *41*, 10375.
  30. Ogliaro, F., de Visser, S. P., and Shaik, S. (2002) The 'push' effect of the thiolate ligand in cytochrome p450: A theoretical gauging, *J. Inorg. Biochem.* *91*, 554.

31. Wang, R., and de Visser, S. P. (2007) How does the push/pull effect of the axial ligand influence the catalytic properties of compound i of catalase and cytochrome p450?, *J. Inorg. Biochem.* 101, 1464.
32. Meunier, B., de Visser, S. P., and Shaik, S. (2004) Mechanism of oxidation reactions catalyzed by cytochrome p450 enzymes, *Chem. Rev.* 104, 3947.
33. Galinato, M. G. I., Spolitak, T., Ballou, D. P., and Lehnert, N. (2011) Elucidating the role of the proximal cysteine hydrogen-bonding network in ferric cytochrome p450cam and corresponding mutants using magnetic circular dichroism spectroscopy, *Biochemistry* 50, 1053.
34. Ueyama, N., Nishikawa, N., Yamada, Y., Okamura, T., and Nakamura, A. (1996) Cytochrome p-450 model (porphinato)(thiolato)iron(iii) complexes with single and double nh center dot center dot center dot s hydrogen bonds at the thiolate site, *J. Am. Chem. Soc.* 118, 12826.
35. Yoshioka, S., Tosha, T., Takahashi, S., Ishimori, K., Hori, H., and Morishima, I. (2002) Roles of the proximal hydrogen bonding network in cytochrome p450(cam)-catalyzed oxygenation, *J. Am. Chem. Soc.* 124, 14571.
36. Voegtle, H. L., Sono, M., Adak, S., Pond, A. E., Tomita, T., Perera, R., Goodin, D. B., Ikeda-Saito, M., Stuehr, D. J., and Dawson, J. H. (2003) Spectroscopic characterization of five- and six-coordinate ferrous-heme complexes. Evidence for heme fe-proximal cysteinyl bond cleavage in the ferrous-heme adducts of the trp-409tyr/phe proximal environment mutants of neuronal nitric oxide synthase, *Biochemistry* 42, 2475.
37. Couture, M., Adak, S., Stuehr, D. J., and Rousseau, D. L. (2001) Regulation of the properties of the heme-heme complexes in nitric-oxide synthase by hydrogen bonding to the proximal cysteine, *J. Biol. Chem.* 276, 38280.
38. Lang, J., Driscoll, D., Gelin, S., Rafferty, S. P., and Couture, M. (2009) Trp180 of endothelial nos and trp56 of bacterial nos modulate sigma bonding of the axial cysteine to the heme, *J. Inorg. Biochem.* 103, 1102.
39. Tejero, J., Biswas, A., Wang, Z.-Q., Page, R. C., Haque, M. M., Hemann, C., Zweier, J. L., Misra, S., and Stuehr, D. J. (2008) Stabilization and characterization of a heme-oxy reaction intermediate in inducible nitric-oxide synthase, *Journal of Biological Chemistry* 283, 33498.
40. Rittle, J., and Green, M. T. (2010) Cytochrome p450 compound i: Capture, characterization, and c-h bond activation kinetics, *Science* 330, 933.
41. Sudhamsu, J., and Crane, B. R. (2006) Structure and reactivity of a thermostable prokaryotic nitric-oxide synthase that forms a long-lived oxy-heme complex, *J. Biol. Chem.* 281, 9623.
42. Kabir, M., Sudhamsu, J., Crane, B. R., Yeh, S. R., and Rousseau, D. L. (2008) Substrate-ligand interactions in geobacillus stearothermophilus nitric oxide synthase, *Biochemistry* 47, 12389.
43. Sreerama, N., Venyaminov, S. Y. U., and Woody, R. W. (1999) Estimation of the number of  $\alpha$ -helical and  $\beta$ -strand segments in proteins using circular dichroism spectroscopy, *Protein Science* 8, 370.
44. Wang, J. L., Rousseau, D. L., Abusoud, H. M., and Stuehr, D. J. (1994) Heme coordination of no in no synthase, *P. Natl. Acad. Sci. USA* 91, 10512.

45. Berry, E. A., and Trumpower, B. L. (1987) Simultaneous determination of hemes-a, hemes-b, and hemes-c from pyridine hemochrome spectra, *Anal. Biochem.* *161*, 1.
46. Dmochowski, I. J., Dunn, A. R., Wilker, J. J., Crane, B. R., Green, M. T., Dawson, J. H., Sligar, S. G., Winkler, J. R., and Gray, H. B. (2002) Sensitizer-linked substrates and ligands: Ruthenium probes of cytochrome p450 structure and mechanism, *Method. Enzymol.* *357*, 120.
47. Schenkma.Jb, Remmer, H., and Estabroo.Rw. (1967) Spectral studies of drug interaction with hepatic microsomal cytochrome, *Mol. Pharmacol.* *3*, 113.
48. Lancaster, K. M., Sproules, S., Palmer, J. H., Richards, J. H., and Gray, H. B. (2010) Outer-sphere effects on reduction potentials of copper sites in proteins: The curious case of high potential type 2 c112d/m121e pseudomonas aeruginosa azurin, *J. Am. Chem. Soc.* *132*, 14590.
49. Schubert, E. M. (1992) Utilizing the evans method with a superconducting nmr spectrometer in the undergraduate laboratory, *Journal of Chemical Education* *69*, 62.
50. Hartings, M. R., Gray, H. B., and Winkler, J. R. (2008) Probing melittin helix-coil equilibria in solutions and vesicles, *J. Phys. Chem. B* *112*, 3202.
51. Porter, T. D. (1994) Mutagenesis at a highly conserved phenylalanine in cytochrome p450 2e1 affects heme incorporation and catalytic activity, *Biochemistry* *33*, 5942.
52. Sabat, J., Stuehr, D. J., Yeh, S. R., and Rousseau, D. L. (2009) Characterization of the proximal ligand in the p420 form of inducible nitric oxide synthase, *J. Am. Chem. Soc.* *131*, 12186.
53. Crane, B. R., Arvai, A. S., Gachhui, R., Wu, C. Q., Ghosh, D. K., Getzoff, E. D., Stuehr, D. J., and Tainer, J. A. (1997) The structure of nitric oxide synthase oxygenase domain and inhibitor complexes, *Science* *278*, 425.
54. Jovanovic, T., Farid, R., Friesner, R. A., and McDermott, A. E. (2005) Thermal equilibrium of high- and low-spin forms of cytochrome p450bm-3: Repositioning of the substrate?, *J. Am. Chem. Soc.* *127*, 13548.
55. Sono, M., Ledbetter, A. P., McMillan, K., Roman, L. J., Shea, T. M., Masters, B. S. S., and Dawson, J. H. (1999) Essential thiol requirement to restore pterin- or substrate-binding capability and to regenerate native enzyme-type high-spin heme spectra in the escherichia coli-expressed tetrahydrobiopterin-free oxygenase domain of neuronal nitric oxide synthase†, *Biochemistry* *38*, 15853.
56. Migita, C. T., Salerno, J. C., Masters, B. S. S., Martasek, P., McMillan, K., and Ikeda-Saito, M. (1997) Substrate binding-induced changes in the epr spectra of the ferrous nitric oxide complexes of neuronal nitric oxide synthase†, *Biochemistry* *36*, 10987.
57. Salerno, J. C., McMillan, K., and Masters, B. S. S. (1996) Binding of intermediate, product, and substrate analogs to neuronal nitric oxide synthase: Ferriheme is sensitive to ligand-specific effects in the l-arginine binding site†, *Biochemistry* *35*, 11839.
58. Tejero, J. S., Biswas, A., Wang, Z. Q., Page, R. C., Haque, M. M., Hemann, C., Zweier, J. L., Misra, S., and Stuehr, D. J. (2008) Stabilization and characterization

of a heme-oxy reaction intermediate in inducible nitric-oxide synthase, *J. Biol. Chem.* 283, 33498.